Localization of Wheeled Mobile Robots from Slip Ratio Estimation with Simple Model

Urara Kono, Hiroshi Fujimoto, Yoichi Hori
The University of Tokyo
5-1-5, Kashiwanoha, Kashiwa, Chiba, 277-8561, Japan
kono.urara20@ae.k.u-tokyo.ac.jp, fujimoto@k.u-tokyo.ac.jp, hori@k.u-tokyo.ac.jp

***Abstract*—This paper proposes a localization method by estimating the slip ratio of wheeled mobile robots. The slip ratio estimator is designed based on the equations of motion. Input torque and encoders data are used, and driving force, vehicle velocity, and slip rate are estimated. This method can estimate the robot's position accurately without visual odometry (VO) when the driving resistance is obtained. When VO is available, even if the obtained driving resistance is different from its true value, instantaneous speed observer updates the resistance and the robot's velocity. The sampling time of torque is very short, which allows us to obtain position estimation much faster than VO. The experiments were conducted with a robot on alumina balls, and the proposed methods showed improvements in the accuracy of localization compared to wheel odometry.**

***Index Terms*—localization, wheeled robots, field robotics**

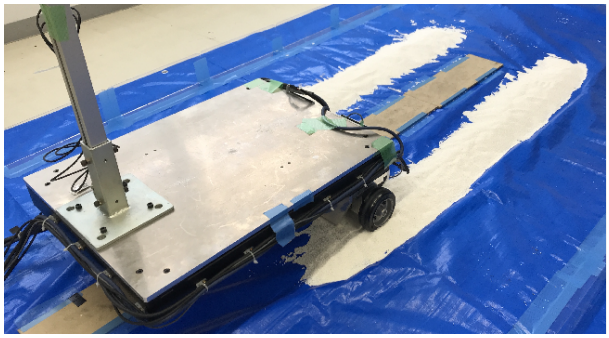

Fig. 1: Wheeled mobile robot

Superscript

$i \in$ l, r Wheel number (l: left, r: right)

Variables

V	Robot's longitudinal velocity
F_{dr}	Driving resistance
N^i	Nominal reaction force on wheel i
F_x^i	Driving force of wheel i
λ^i	Slip ratio of wheel i
μ^i	Friction coefficient at wheel i
ω^i	Angular velocity of motor side of wheel i
$\dot{\omega}^i$	Angular acceleration of motor side of wheel i
T^i	Motor torque of wheel i
V_ω^i	Velocity of wheel i

I. Introduction

Wheeled mobile robots (WMRs) are used in various situations, including planetary explorations, disaster sites, and delivery services. They also show improvements in a power-assisted mode for human-friendly mobile carts [1]. Real-time localization of WMRs is important to explore unknown, non-homogeneous terrain safely and efficiently. Inertial measurement unit (IMU), wheel odometry (WO), and visual odometry (VO) have been utilized for the localization.

In planetary exploration, NASA's Mars rovers have employed similar localization methods: WO measures the distance the rover traversed from the encoders, and IMU provides tilt estimates and attitudes [2]. WO is inexpensive, accurate in short-term, and obtained at very high sampling rates [3]. In the Mars Exploration Rover (MER) mission, when a rover ran at the flat ground for 2 km, the accumulated error was only 3% [4]. However, WO suffers from errors due to wheel slip on uneven terrains and slippery surfaces [5]. To tackle the errors, VO is used on WMRs. It is the vision-based method and has been heavily used on WMRs including Mars rovers [6]. Although VO works well, errors still exist as cameras cannot see well in dark places or feature-less terrains and can cause feature matching to fail. For real-time slip ratio estimation and control, VO is not suitable [7] for its low sampling rate compared to internal sensors such as encoders and IMUs.

There has been a large amount of work to estimate the slip ratio of WMRs. [8] and [9] fused acceleration sensors, gyros, and encoders in extended Kalman filter. For the slip ratio estimation of skid-steered mobile robots, non-linear sliding mode observer was used in [10] and IMU-based nonlinear Kalman filter was presented in [11]. [12] proposed estimating slip using motor current, IMU, encoders, and potentiometers, but it needs some calibration movements when no absolute positioning system is available. This paper is different from these conventional methods in that it does not use IMU. Terramechanics have worked on slip ratio estimation by making models of the ground and the wheel [13], [14]. However, soil parameters need to be known to use terramechanics models. Current research tries to estimate the parameters, but that method needs heavy computation [15].

This paper proposes a new localization method by estimating slip ratio from the input torque and the motors' encoders on the wheels. It is model-based and derives the motion equations

2021 IEEE International Conference on Mechatronics (ICM) | 978-1-7281-4442-9/21/$31.00 ©2021 IEEE | DOI: 10.1109/ICM46511.2021.9385671

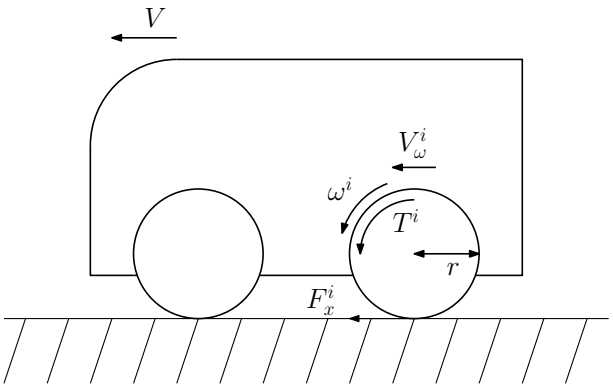

Fig. 2: Robot model.

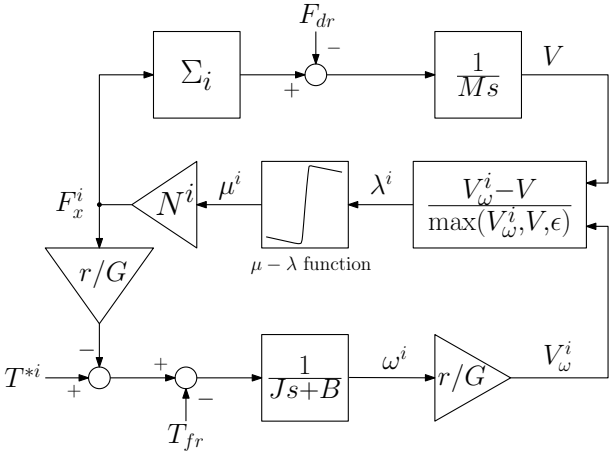

Fig. 3: Block diagram of the plant.

TABLE I: PLANT MODEL PARAMETERS

Description	Symbol	Value
Inertia from motor side	J	$4.8 \times 10^{-6}\,\mathrm{kg\,m^2}$
Viscous coefficient from motor side	B	$6.3 \times 10^{-5}\,\mathrm{N\,s/m^2}$
Coulomb friction	T_{fr}	$2.3 \times 10^{-2}\,\mathrm{N\,m}$
Wheel radius	r	$5.0 \times 10^{-2}\,\mathrm{m}$
Gear ratio	G	31
Robot mass	M	$30.6\,\mathrm{kg}$

of the WMR. This method is robust to the noise because it does not integrate the acceleration from the IMU, which would contain large offsets. The driving force is estimated from the disturbance observer [16], and the robot velocity is calculated with the angular velocity of the encoders and the input torque.

The slip ratio estimator was first developed on electric vehicles (EVs) with in-wheel motors by [17], [18] and used for the driving force control of EVs [19], [20]. It is much less computationally demanding than VO and will be useful for robots with limited processing. Since the torque response of motors is short – a few milliseconds, the slip ratio can be obtained at much higher rates than VO. The proposed method improves the localization accuracy while driving between keyframes or waypoints. The estimated slip will be helpful for real-time slip control and could potentially be used for WMRs running in the darkness or feature-less terrains where VO is not available if the value of the driving resistance is known with some accuracy.

The rest of this paper is organized as follows: In Section II, the model of the WMR is described. The estimation method is presented in Section III. Fusion of slip ratio estimator and VO using instantaneous speed observer is proposed in Section IV. Experiments are described in Section V. Section VI concludes this paper.

II. Dynamic Model of Robot

Fig. 2 shows the wheels and the body model and their longitudinal motion is described as

$$J\dot{\omega}^i = T^i - (r/G)F_x^i - B\omega^i - T_{fr}, \tag{1}$$

$$M\dot{V} = \Sigma F_x^i - F_{dr}, \tag{2}$$

$$V_\omega^i = (r/G)\omega^i. \tag{3}$$

Plant model parameters are shown in Table I. Driving resistance F_{dr} is mainly composed of a constant value, the rolling resistance. Since WMRs run at very lower speed than vehicles, air resistance is neglected. F_{dr} also includes modeling errors such as forces resulted from the complicated wheel contact with the terrain and the transmission efficiency of motor gears. Equation (1) considers viscous friction and Coulomb friction, which were minor and neglected for slip ratio estimation for EVs [17], [18]. On WMRs, these terms should be taken into account for their small mass and torque compared to EVs. The slip ratio λ^i is defined as

$$\lambda^i = \frac{V_\omega^i - V}{\max(V_\omega^i, V, \epsilon)}. \tag{4}$$

ϵ is the minute value to avoid zero denominator. In this paper, the robot is running straight, and the driving force is described as

$$F_x^i = \mu^i N^i. \tag{5}$$

The block diagram of the plant is presented in Fig. 3. The driving force F_x^i is estimated using driving force observer (DFO) [16] shown in Fig. 4, which is derived from (1). T and ω are low-pass filtered so that they are in the same phase with $\dot{\omega}$.

III. Slip Ratio Estimation Method

In the Subsections III-A and III-B, the slip ratio estimator for acceleration mode [17] and deceleration [18] mode is presented, respectively. These two modes are switched by looking at the value of $\max(V_\omega, V, \epsilon)$ in (4).

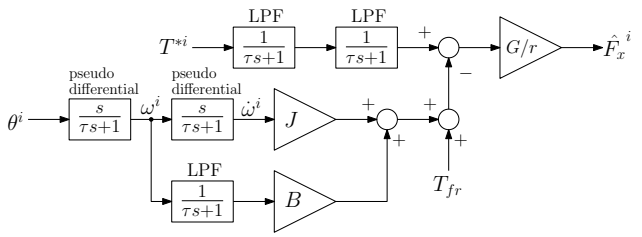

Fig. 4: The diagram of DFO. θ^i is the angle obtained from the encoder. $\tau = 10\,\mathrm{ms}$.

A. Acceleration Mode $(\max(V_\omega, V, \epsilon) = V_\omega)$

The slip ratio estimation for acceleration mode was proposed by [17]. In this mode, $\max(V_\omega, V, \epsilon) = V_\omega$. By differentiating (4) and using (1), the differential equation of λ is obtained as follow:

$$\dot{\lambda} = (1-\lambda)\frac{\dot{\omega}}{\omega} - \frac{1}{M(r/G)\omega}(\Sigma F_x^i - F_{dr}) \tag{6}$$

The slip ratio estimator is designed by putting hats, which mean estimated values, on the unmeasured terms ΣF_x^i and F_{dr} in (6):

$$\dot{\hat{\lambda}} = (1-\hat{\lambda})\frac{\dot{\omega}}{\omega} - \frac{1}{M(r/G)\omega}(\Sigma \hat{F}_x^i - \hat{F}_{dr}) \tag{7}$$

$\hat{F}_x^i$ is obtained from DFO. $\hat{F}_{dr}$ contains not only driving resistance but also modeling errors or disturbances.

When $\hat{\lambda}^i$ converges, the estimation error defined as (8) will also converge.

$$e^i = \lambda^i - \hat{\lambda}^i. \tag{8}$$

By subtracting (7) from (6), the differential equation of e^i is obtained:

$$\dot{e}^i = -\frac{\dot{\omega}^i}{\omega^i}e^i + \frac{F_{dr} - \hat{F}_{dr}}{(r/G)M\omega^i}. \tag{9}$$

If $F_{dr} = \hat{F}_{dr}$ and $\dfrac{\dot{\omega}^i}{\omega^i} > 0$, the estimation error will converge to zero. When $F_{dr} \neq \hat{F}_{dr}$ and $\dfrac{\dot{\omega}^i}{\omega^i} > 0$, e^i will converge to a non-zero value. The estimated robot velocity is calculated by

$$\hat{V} = (1-\hat{\lambda}^i)V_\omega^i. \tag{10}$$

B. Deceleration Mode $(\max(V_\omega, V, \epsilon) = V)$

The slip ratio estimation for deceleration mode was proposed by [18]. When the robot is braking, $\max(V_\omega, V, \epsilon) = V$. The robot does not have mechanical brakes and stops by velocity control. By differentiating (4) and using (2), (11) is obtained.

$$\dot{\lambda} = (1+\lambda)\frac{\dot{\omega}}{\omega} - \frac{(1+\lambda)^2}{M(r/G)\omega}(\Sigma F_x^i - F_{dr}). \tag{11}$$

Based on (11), the slip ratio estimator for deceleration mode is designed:

$$\dot{\hat{\lambda}} = (1+\hat{\lambda})\frac{\dot{\omega}}{\omega} - \frac{(1+\hat{\lambda})^2}{M(r/G)\omega}(\Sigma \hat{F}_x^i - \hat{F}_{dr}). \tag{12}$$

By subtracting (12) from (11), the differential equation of e^i is obtained:

$$\dot{e}^i = \left\{\frac{\dot{\omega}^i}{\omega^i} - \left(\frac{\Sigma F_x^i - F_{dr}}{M(r/G)\omega^i}\right)(\lambda^i + \hat{\lambda}^i + 2)\right\} e^i. \tag{13}$$

Using $\dot{V}_\omega^i, V_\omega^i$, and $\dot{V}$, (13) can also be written as

$$\dot{e}^i = \left(\frac{\dot{V}_\omega^i}{V_\omega^i} - \frac{\dot{V}}{V_\omega^i}(2 + \lambda^i + \hat{\lambda}^i)\right) e^i. \tag{14}$$

The error e^i will converge if $\dot{V}_\omega^i - \dot{V}^i(2 + \lambda^i + \hat{\lambda}^i) < 0$. The estimated robot velocity is calculated by

$$\hat{V} = \frac{V_\omega^i}{(1+\hat{\lambda}^i)}. \tag{15}$$

IV. Updates of Driving Resistance, Velocity, and Position by Instantaneous Speed Observer

VO is implemented in most current wheeled robots. In order to estimate the position more accurately with VO, the authors propose a method using instantaneous speed observer [21]. The instantaneous speed observer is a method that, when different sensor values are obtained at different sampling times T_1, T_2 $(T_1 > T_2)$, updates an estimator running every T_2 with the information obtained every T_1. In this case, position estimation from VO is obtained every $T_1 = 1\,\mathrm{s}$, and the slip ratio estimator described in Section III is running every $T_2 = 1\,\mathrm{ms}$. This time, the slip ratio estimator (Section III) is run assuming that the driving resistance is a known constant value. However, even if the value is different from the actual one, an approximate value can be obtained from this instantaneous speed observer. Once the approximate value is known, the slip ratio estimator will converge based on (9), (14). and follow the true value even as the driving resistance changes.

If $T_1/T_2 = K$, time t is expressed as $t = mT_1 + kT_2 (1 \leq k \leq K,\ m, k \in \mathbb{Z})$ denoted by $[m, k]$. At the short sampling point T_2, the slip rate and position are estimated as follows:

$$\hat{\lambda}[m,k] = \hat{\lambda}[m,k-1] + \frac{T_2}{2}(\dot{\hat{\lambda}}[m,k] + \dot{\hat{\lambda}}[m,k-1]), \tag{16}$$

$$\hat{x}[m,k] = \hat{x}[m,k-1] + \frac{T_2}{2}(\hat{V}[m,k] + \hat{V}[m,k-1]). \tag{17}$$

At the long sampling point T_1, the position information x_{VO} is obtained from VO with good accuracy. Δx, the difference between x_{VO} and $\hat{x}[m,k]$ is calculated every T_1. We consider that Δx is caused by two factors: ΔV, the initial error of the robot's velocity at the start of the estimation in the interval of T_1, and ΔF_{dr}, the error of the driving resistance assumed in that interval. The causes of Δx are distributed to these variables in the ratio γ_1 and γ_2 $(\gamma_1 + \gamma_2 = 1)$, respectively.

$$\gamma_1 \Delta x = T_1 \Delta V, \tag{18}$$

$$\gamma_1 \Delta x = -\frac{T_1^2}{2M}\Delta F_{dr}. \tag{19}$$

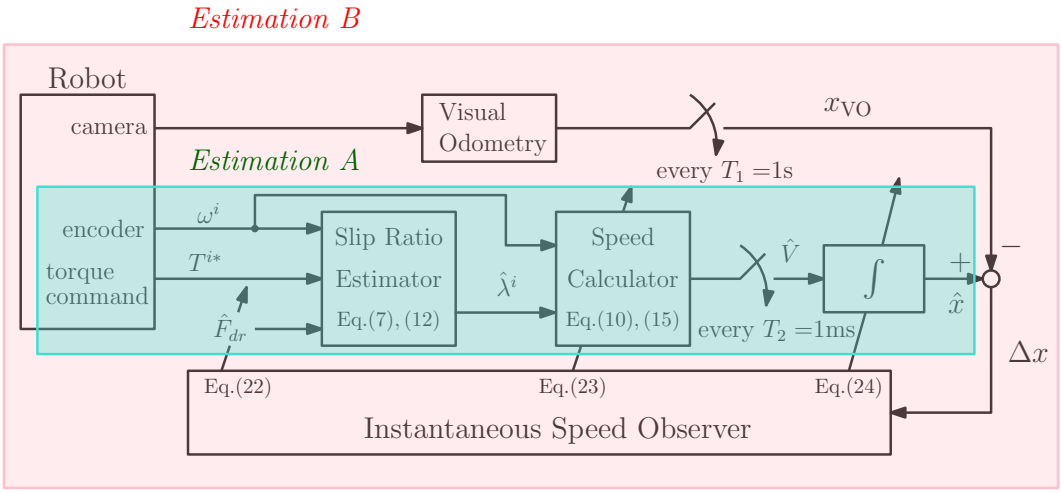

Fig. 5: The overview of the whole system. Slip is estimated from encoder data, torque command, and driving resistance model. Instantaneous speed observer updates $\hat{V}$ and F_{dr} every T_2. Green part and red part were used in Estimation A and B, respectively.

These equations give the amount of correction in the next interval as follows:

$$\Delta V = \frac{1}{T_1}\gamma_1 \Delta x, \tag{20}$$

$$\Delta F_{dr} = -\frac{2M}{T_1^2}\gamma_2 \Delta x. \tag{21}$$

$\hat{F}_{dr}[m+1]$ and $\hat{V}[m+1,0]$ are updated as follows:

$$\hat{F}_{dr}[m+1] = \hat{F}_{dr}[m] - \Delta F_{dr}, \tag{22}$$

$$\hat{V}[m+1,0] = \hat{V}[m,K] - \Delta V - \frac{T_1}{M}\Delta F_{dr}. \tag{23}$$

$\hat{\lambda}[m+1,0]$ is also updated from (23) using (4). The estimated position from slip ratio estimator is updated to x_{VO} at sampling rate T_1 and described as

$$\hat{x}[m+1,0] = x_{\mathrm{VO}}[m+1]. \tag{24}$$

The convergence condition is determined from the following matrix [21]:

$$\begin{pmatrix} 1 & \frac{T_1}{M} \\ 0 & 1 \end{pmatrix} \left(I - \begin{pmatrix} T_1 & 0 \\ 0 & \frac{T_1^2}{2M} \end{pmatrix}^{-1} \begin{pmatrix} \gamma_1 \\ \gamma_2 \end{pmatrix} \begin{pmatrix} T_1 & \frac{T_1^2}{2M} \end{pmatrix} \right)$$
$$= \begin{pmatrix} -\gamma_2 & \frac{T_1}{2M}(2-\gamma_1-2\gamma_2) \\ -\frac{2M}{T_1}\gamma_2 & \gamma_1 \end{pmatrix}. \tag{25}$$

I is unit matrix. If the eigenvalues of the matrix (25) are within unit circle in the discrete-time system, the observer will converge. As for this system, any γ_1 and γ_2 ($0 < \gamma_1 < 1, 0 < \gamma_2 < 1, \gamma_1 + \gamma_2 = 1$) meets this condition.

When this observer updates variables every T_1, the values in (9) and (14) also change and e^i restarts converging. These two differential describe the dynamics within T_1. Therefore, the convergence condition for slip ratio estimator (9),(14) and that for instantaneous speed observer (25) will not conflict to each other.

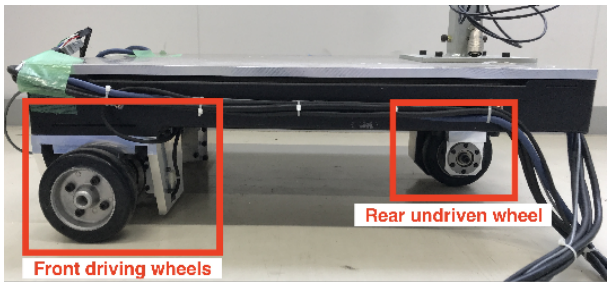

Fig. 6: Robot wheels

The block diagram of the whole localization system is represented in Fig. 5.

V. Experiments

The WMR presented in Fig. 1 was used to validate the proposed methods. The robot has two driving wheels in front and one undriven wheel in the rear as shown in Fig. 6. The undriven wheel is assumed not to slip, and the true velocity of the robot is obtained from the undriven wheel's velocity. Table I presents the robot's physical parameters. The resolution of the encoder is 14 bit. The two driving wheels ran on alumina balls whose diameters are 2 mm. The undriven wheel ran on the boards so that it would smoothly rotate without making a slip.

The wheels' motor were controlled with their velocity feedback. The cutoff frequency for the pseudo differential of encoder data was 500 rad/s ($\tau = 2$ ms). The PI gains K_p, K_i were set so that the pole of the speed feedback was $\omega_c = 10$ rad/s. The cutoff frequency of pseudo differential to calculate ω and $\dot{\omega}$ for the input of slip ratio estimator was 100 rad/s ($\tau = 10$ ms).

In this experiment, the robot running at 0.1 m/s accelerated suddenly, making a big slip. When the robot was braked,

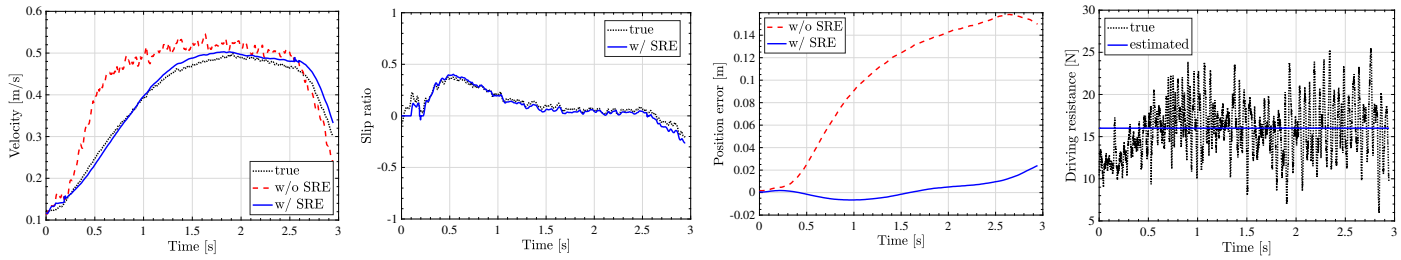

(a) Velocity. (b) Slip ratio. (c) Position error. (d) Driving resistance.

Fig. 7: *Estimation A*. Only slip ratio estimator (SRE) with the accurate average value of driving resistance ($\hat{F}_{dr} = 16\,\mathrm{N}$). The green region in Fig. 5.

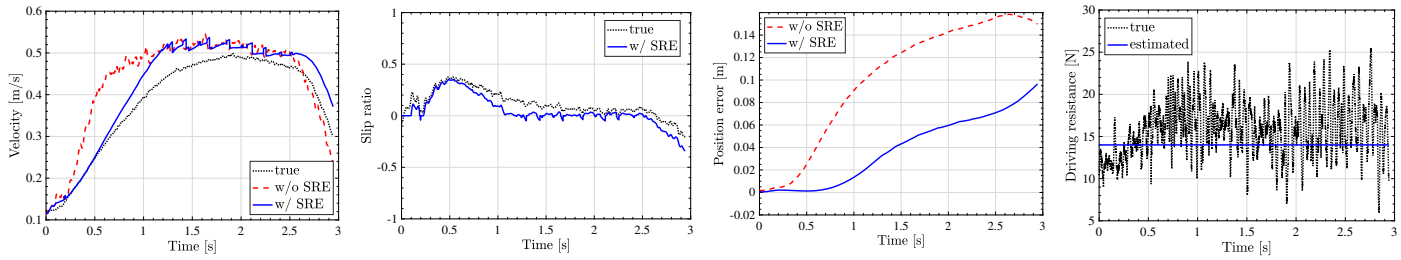

(a) Velocity. (b) Slip ratio. (c) Position error. (d) Driving resistance.

Fig. 8: *Estimation A*. Only slip ratio estimator (SRE) worked with inaccurate driving resistance ($\hat{F}_{dr} = 14\,\mathrm{N}$). The green region in Fig. 5.

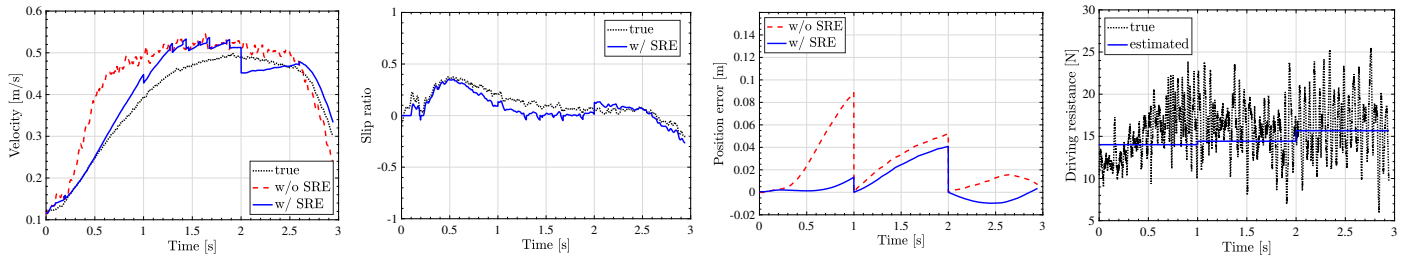

(a) Velocity. (b) Slip ratio. (c) Position error. (d) Driving resistance.

Fig. 9: *Estimation B*. The hybrid of slip ratio estimation (SRE) and VO by instantaneous speed observer using driving resistance with initial error ($\hat{F}_{dr0} = 14\,\mathrm{N}$). The red region in Fig. 5.

it slipped again, and the slip rate was negative. Slip ratio estimator started at $V_\omega = 0.15\,\mathrm{m/s}$. Even if the estimator starts at different velocity, the slip ratio estimator will converge by (9),(14).

Two kinds of estimation were conducted. The first method is slip ratio estimator (Section III), which is depicted as red region in Fig. 5. We name this method as *Estimation A*. The results of this method are stated in Section V-A. The other method uses both slip ratio estimator (Section III) and instantaneous speed observer (Section IV), which is depicted as green region in Fig. 5. We name this method as *Estimation B*. The results of this method are stated in Section V-B.

A. Slip Ratio Estimator with constant F_{dr} (Estimation A)

In this estimation, VO information was not available, and only slip ratio estimator was used. The driving resistance was assumed to be constant.

First, *Estimation A* was conducted with a constant value of $\hat{F}_{dr} = 16\,\mathrm{N}$ and the results are shown in Fig. 7. The average value of the driving resistance was known accurately as shown in Fig. 7d. The robot's position was estimated very accurately compared to WO plotted with red lines even without VO.

Next, *Estimation A* was conducted with $\hat{F}_{dr} = 14\,\mathrm{N}$, a slight deviation from the true average value of $16\,\mathrm{N}$. The results are shown in Fig. 8. From Fig. 8c, the position error of *Estimation A* (blue line) was smaller than that of WO (red line), but it accumulatd errors continuously.

B. Slip Ratio Estimator and Instantaneous Speed Observer with inaccurate initial value F_{dr0} (Estimation B)

In this subsection, VO was fused with slip ratio estimator by instantaneous speed observer to minimize the position error caused by the deviation of driving resistance. The initial value of driving resistance $\hat{F}_{dr0}$ was $14\,\mathrm{N}$, and γ_1 and γ_2 were both set to 0.5. The estimation results are shown in Fig. 9. Every $T_1 = 1\,\mathrm{s}$, instantaneous speed observer updated $\hat{V}$ and $\hat{F}_{dr}$, and estimated values changed at the same time. From Fig. 9d, the driving resistance approached its true average value.

VI. Conclusion

This paper proposed localization of WMRs by estimating slip ratio from proprioceptive information such as encoders and input torque. From the equation of motion, differential equations for estimating slip rates are obtained. Even if there is a little error in the driving resistance value, the equations will converge. This method allowed us to obtain better accuracy than WO. We also proposed a method of using an instantaneous speed observer to fuse slip ratio estimator with VO. In the instantaneous speed observer, the causes of position error are considered the errors of estimated velocity and driving resistance. These two terms are updated every time VO is obtained.

VO is essentially blind driving between waypoints or keyframes. Therefore, with the proposed method, position estimation is obtained with high accuracy and much faster than the VO. The proposed methods can reduce the dependence on VO for robots with limited computation or as a backup.

As future work, lateral slip could be estimated by formulating the motion equations in the lateral direction.

References

[1] R. Kitayoshi and H. Fujimoto, "Human-friendly acceleration control for mobile cart with torque sensor built in driving shaft," *IEEJ Journal of Industry Applications*, vol. 9, no. 6, pp. 629–636, 2020.

[2] J. P. Grotzinger, J. Crisp, A. R. Vasavada, R. C. Anderson, C. J. Baker, R. Barry, D. F. Blake, P. Conrad, K. S. Edgett, B. Ferdowski, R. Gellert, J. B. Gilbert, M. Golombek, J. Gómez-Elvira, D. M. Hassler, L. Jandura, M. Litvak, P. Mahaffy, J. Maki, M. Meyer, M. C. Malin, I. Mitrofanov, J. J. Simmonds, D. Vaniman, R. V. Welch, and R. C. Wiens, *Mars Science Laboratory mission and science investigation*, 2012, vol. 170, no. 1-4.

[3] J. Borenstein, H. R. Everett, L. Feng, and D. Wehe, "Mobile robot positioning: Sensors and techniques," *Journal of Robotic Systems*, vol. 14, no. 4, pp. 231–249, 1997.

[4] J. J. Biesiadecki, P. C. Leger, and M. W. Maimone, "Tradeoffs between directed and autonomous driving on the Mars exploration rovers," *International Journal of Robotics Research*, vol. 26, no. 1, pp. 91–104, 2007.

[5] S. A. Mohamed, M. H. Haghbayan, T. Westerlund, J. Heikkonen, H. Tenhunen, and J. Plosila, "A Survey on Odometry for Autonomous Navigation Systems," *IEEE Access*, vol. 7, pp. 97 466–97 486, 2019.

[6] M. Maimone, Y. Cheng, and L. Matthies, "Two years of visual odometry on the Mars Exploration Rovers," *Journal of Field Robotics*, vol. 24, no. 3, pp. 169–186, 2007.

[7] Y. P. Li, M. H. Ang, and W. Lin, "Slip modelling, detection and control for redundantly actuated wheeled mobile robots," *IEEE/ASME International Conference on Advanced Intelligent Mechatronics, AIM*, pp. 967–972, 2008.

[8] C. C. Ward and K. Iagnemma, "Model-based wheel slip detection for outdoor mobile robots," *Proceedings - IEEE International Conference on Robotics and Automation*, no. April, pp. 2724–2729, 2007.

[9] M. Seyr and S. Jakubek, "Proprioceptive navigation, slip estimation and slip control for autonomous wheeled mobile robots," *2006 IEEE Conference on Robotics, Automation and Mechatronics*, 2006.

[10] Z. B. Song, Y. H. Zweiri, K. Althoefer, and L. D. Seneviratne, "Nonlinear observer for slip estimation of tracked vehicles," *13th Annual International Conference on Mechatronics and Machine Vision in Practice 2006*, no. May, pp. 13–23, 2006.

[11] J. Yi, J. Zhang, D. Song, and S. Jayasuriya, "IMU-based localization and slip estimation for skid-steered mobile robots," *IEEE International Conference on Intelligent Robots and Systems*, no. October 2007, pp. 2845–2850, 2007.

[12] L. Ojeda, D. Cruz, G. Reina, and J. Borenstein, "Current-based slippage detection and odometry correction for mobile robots and planetary rovers," *IEEE Transactions on Robotics*, vol. 22, no. 2, pp. 366–378, 2006.

[13] L. Ding, H. Gao, Z. Deng, K. Yoshida, and K. Nagatani, "Slip ratio for lugged wheel of planetary rover in deformable soil: Definition and estimation," *2009 IEEE/RSJ International Conference on Intelligent Robots and Systems, IROS 2009*, pp. 3343–3348, 2009.

[14] K. Yoshida and H. Hamano, "Motion dynamics of a rover with slip-based traction model," in *Proceedings - IEEE International Conference on Robotics and Automation*, vol. 3, no. May, 2002, pp. 3155–3160.

[15] Shamrao, C. Padmanabhan, S. Gupta, and A. Mylswamy, "Estimation of terramechanics parameters of wheel-soil interaction model using particle filtering," *Journal of Terramechanics*, vol. 79, pp. 79–95, 2018.

[16] Y. Hori, "Future vehicle driven by electricity and control - Research on four-wheel-motored "UOT Electric March II"," *IEEE Transactions on Industrial Electronics*, vol. 51, no. 5, pp. 954–962, 2004.

[17] K. Fujii and H. Fujimoto, "Traction control based on slip ratio estimation without detecting vehicle speed for electric vehicle," in *Fourth Power Conversion Conference-NAGOYA*, 2007.

[18] T. Suzuki and H. Fujimoto, "Slip ratio estimation and regenerative brake control without detection of vehicle velocity and acceleration for electric vehicle at urgent brake-turning," in *2010 11th IEEE International Workshop on Advanced Motion Control (AMC)*. IEEE, mar 2010, pp. 273–278.

[19] H. Fujimoto, K. Fujii, and N. Takahashi, "Vehicle stability control of electric vehicle with slip-ratio and cornering stiffness estimation," *IEEE/ASME International Conference on Advanced Intelligent Mechatronics, AIM*, no. 1, pp. 2–7, 2007.

[20] K. Maeda, H. Fujimoto, and Y. Hori, "Four-wheel Driving-force Distribution Method for Instantaneous or Split Slippery Roads for Electric Vehicle," *Automatika*, vol. 54, no. 1, pp. 103–113, jan 2013.

[21] Y. Konno and Y. Hori, "Instantaneous Speed Observer with Improved Disturbance Rejection Performance based on Higher Order Dynamics." *IEEJ Transactions on Industry Applications*, vol. 112, no. 6, pp. 539–544, 1992.